Front. Mech. Eng. 2016, 11(2): 144–158
DOI 10.1007/s11465-016-0391-0

RESEARCH ARTICLE

Mingfeng WANG, Marco CECCARELLI, Giuseppe CARBONE

A feasibility study on the design and walking operation of a biped locomotor via dynamic simulation

Abstract A feasibility study on the mechanical design and walking operation of a Cassino biped locomotor is presented in this paper. The biped locomotor consists of two identical 3 degrees-of-freedom tripod leg mechanisms with a parallel manipulator architecture. Planning of the biped walking gait is performed by coordinating the motions of the two leg mechanisms and waist. A three-dimensional model is elaborated in SolidWorks® environment in order to characterize a feasible mechanical design. Dynamic simulation is carried out in MSC.ADAMS® environment with the aims of characterizing and evaluating the dynamic walking performance of the proposed design. Simulation results show that the proposed biped locomotor with proper input motions of linear actuators performs practical and feasible walking on flat surfaces with limited actuation and reaction forces between its feet and the ground. A preliminary prototype of the biped locomotor is built for the purpose of evaluating the operation performance of the biped walking gait of the proposed locomotor.

Keywords feasibility study, biped locomotor, biped walking, mechanical design, dynamic simulation, tripod leg mechanism, 3-UPU parallel manipulator

1 Introduction

Legged locomotion has a number of advantages compared with conventional wheeled and tracked locomotion, such as better mobility, obstacle overcoming ability, energy efficiency, compliant motion, and achievable speed, especially when it operates in a rough or unconstructed environment [1].

As a hot topic in legged walking machines, biped locomotors have attracted the interest of many research communities in the past decades. As a result, several prototypes have been built in the laboratory frames, even for specific application tasks [2,3]. Most of the existing biped locomotors are based on leg designs with human-like architectures that feature serial chain solutions, such as ASIMO [4], HUBO [5], HRP [6], and so on. However, compared with serial mechanisms, parallel mechanisms are well known for having better performance in terms of dynamic behavior, accuracy, and ratio of payload to own weight; thus, they have been widely studied in both the industry and academia [7,8]. Nevertheless, there are very few works investigating parallel mechanisms, especially those with less than 6 degrees-of-freedom (DOFs), for leg designs in biped locomotors. WL-16 (Waseda Leg-No.16), the world's first dynamic biped walking locomotor carrying an adult human, is based on leg designs with Gough-Stewart parallel mechanisms [9]. Wang et al. [10] have proposed a quadruped/biped reconfigurable walking locomotor based on four 3-UPU parallel mechanisms (U and P stand for universal and prismatic pairs, respectively), which are converted into two 6-SPU parallel mechanisms (S stands for spherical pair) for biped walking. Ceccarelli and Carbone [11] have investigated the possibility of using parallel mechanisms with less than 6 DOFs for leg designs as inspired by the human leg muscular system. Pan and Gao [12] have presented a new hexapod walking robot for situations when a nuclear disaster happens and this work is based on leg designs of 3-DOF parallel mechanisms.

At the Laboratory of Robotics and Mechatronics (LARM) in Cassino, a research line is devoted to building a novel biped locomotor that is based on leg designs with 3-DOF parallel mechanisms. A preliminary version of the proposed tripod leg mechanism has been presented in

Received January 8, 2016; accepted May 7, 2016

Mingfeng WANG (✉)
School of Mechanical and Electrical Engineering, Central South University, Changsha 410083, China; Laboratory of Robotics and Mechatronics (LARM), DICeM, University of Cassino and South Latium, Cassino 03043, Italy
E-mail: wang@unicas.it

Marco CECCARELLI, Giuseppe CARBONE
Laboratory of Robotics and Mechatronics (LARM), DICeM, University of Cassino and South Latium, Cassino 03043, Italy

Ref. [13] with kinematic characteristics analysis for operation performance evaluation and design purposes. Then, a corresponding preliminary prototype has been built and preliminary experimental experiences have been reported in Ref. [14] with regard to the performance of predefined movements with an isosceles trapezium trajectory. The architecture of the proposed tripod leg mechanism has also been investigated for other applications in Refs. [15–17] based on its significant advantages in being a fairly simple structure with closed-form kinematics, large workspace, and more convenient control as compared with 6-DOF parallel mechanisms.

In this paper, the mechanical design problem of the proposed biped locomotor is presented with the aim of conceiving a biped locomotor by using tripod leg mechanisms. A three-dimensional (3D) model is elaborated in SolidWorks® environment to check the easy-operation high-payload features of the proposed locomotor. A planning of biped walking gait is proposed by coordinating the motions of the two leg mechanisms and the waist. The dynamic simulation of biped walking is carried out in MSC.ADAMS® environment to characterize and evaluate the operation performance of the designed locomotor. A preliminary prototype of the biped locomotor is then built and tested with the proposed walking operation in the air.

2 A biped locomotor with 2-tripod leg mechanisms

A 3D model of the proposed biped locomotor is designed in SolidWorks® environment, as shown in Fig. 1(a). The biped locomotor consists of two tripod leg mechanisms and a waist, on which the two leg mechanisms are installed. For each tripod leg mechanism, between the waist and foot, there are three identical limbs consisting of three linear actuators with U-joints at each end. The kinematic scheme of a 3-UPU parallel manipulator as a tripod leg mechanism is shown in Fig. 1(b).

In Fig. 1(b), the position vectors of points A_i ($i=1,2,3$) with respect to base coordinate frame A: O-xyz and B_i ($i=1,2,3$) with respect to moving coordinate frame B: P-uvw (the origins O and P are placed at the corresponding triangle's center), can be written respectively as

$$ {}^{A}\boldsymbol{a}_i = [a_{ix}, a_{iy}, 0]^{\mathrm{T}},\ {}^{B}\boldsymbol{b}_i = {}^{A}\boldsymbol{b}_i = [b_{ix}, b_{iy}, 0]^{\mathrm{T}} \tag{1} $$

where a superscript indicates the reference coordinate frame in which a vector is expressed.

In addition, Points A_i ($i=1,2,3$) lie on an equilateral triangle in the O-xy plane at a radial distance of r_a from Point O, and B_i ($i=1,2,3$) lie on an equilateral triangle in the P-uv plane at a radial distance of r_b from Point P. Furthermore, given that vectors $\boldsymbol{a}_i$ and $\boldsymbol{b}_i$ are constants and their norms are r_a and r_b, respectively, their difference, which is defined as vector $\boldsymbol{c}_i$, is a constant too and its norm is obtained as $c = r_a - r_b$. Hence, a vector-loop equation can be obtained for each limb as

$$ \boldsymbol{l}_i = \boldsymbol{p} + \boldsymbol{b}_i - \boldsymbol{a}_i = \boldsymbol{p} - \boldsymbol{c}_i, \tag{2} $$

where $\boldsymbol{l}_i$ denotes the vector along the prismatic joint axis from A_i to B_i for limb i.

For the inverse kinematics, the length of each limb l_i can be computed according to the given position vector $\boldsymbol{p}$. The solution can be obtained by dot-multiplying Eq. (2) with itself and taking the square root as

$$ l_i = \pm\sqrt{(p_x - c_{ix})^2 + (p_y - c_{iy})^2 + p_z^2} \ \text{ for } i = 1,2,3, \tag{3} $$

where only the positive root can be obtained in the presented leg mechanism, while the negative root cannot be obtained unless reassembling the mechanism.

Furthermore, in order to improve the compactness of the

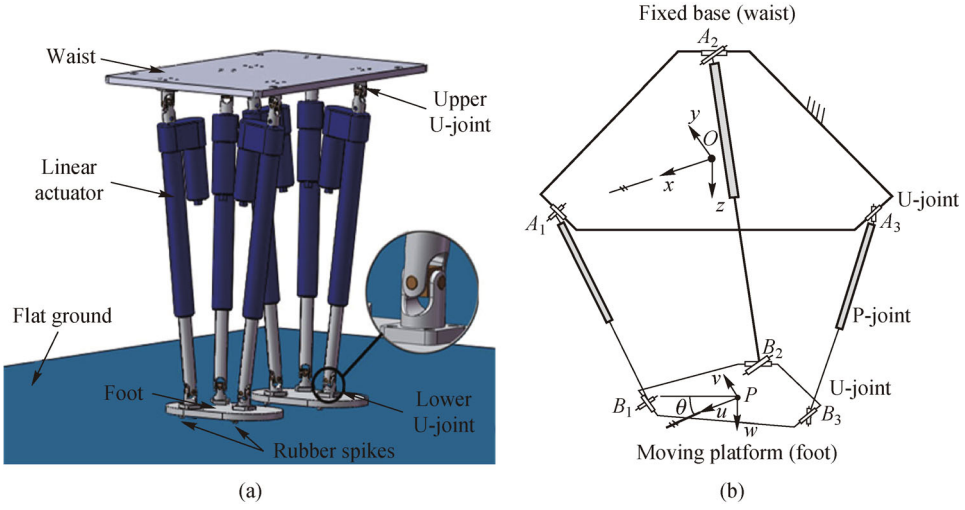

Fig. 1 Design of the Cassino biped locomotor: (a) 3D model; (b) kinematic scheme

proposed biped locomotor, the male parts of the lower U-joints are designed as the bottom part of the rod of each linear actuator. The assembly of lower six U-joints is shown in Fig. 1(a) with a zoomed view. For each leg mechanism, the upper and lower three U-joints are installed in an equilateral triangle arrangement with one ahead and other two rears, as shown in Fig. 2, where the three inner revolute axes are installed pointing to the centers of the triangles with radiuses r_a and r_b, respectively. In order to guarantee that the feet possess pure translational motion, the two U-joints in each limb are arranged with the two outer revolute joint axes being parallel to each other and the two inner revolute joint axes being parallel to one another, as suggested in Ref. [15]. In addition, rubber spikes at the bottom of feet are added to absorb landing impacts when the feet land onto the ground during biped walking.

The main design specifications of the locomotor model are listed in Tables 1 and 2, in accordance with the dimension parameters in Fig. 3. The distance between the upper U-joints and waist is equal to the distance between the lower U-joints and feet, and it is denoted as D_{uw}= D_{uf}. The distance between the two U-joints in each limb, namely, the length of each linear actuator, is indicated as L_i (i = 1, 2, …, 6). The initial value of L_i is set as L_{i0}, which determines the initial dimension of the design configuration given as length (L) ×width (W) ×height (H) in Tables 1 and 2. The lengths of the tube and rod in each linear actuator and its stroke are represented by L_t, L_r and L_s, respectively. The displacement ΔL_i of each linear actuator can be expressed as

$$\Delta L_i = L_i - L_{i0}. \tag{4}$$

The manufacturing feasibility of the mechanical design of the proposed biped locomotor is ensured by using light materials (e.g., aluminum alloy) for the waist and feet, and commercial components (like universal joints and linear actuators) for the structure. Those components have been modelled properly in the proposed CAD design in Figs. 1 and 3 even for simulation purposes.

3 Characterization of walking gait with waist swinging

A scheme for the motion planning of the biped locomotor walking gait is shown in Fig. 4, referring to a horizontal plane. The planning of the walking gait is based on the coordination of the two legs' motions with the waist swinging.

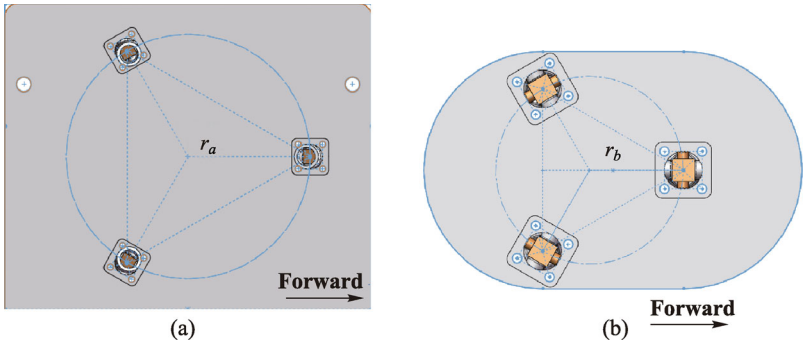

Fig. 2 The arrangement of U-joints: (a) On the waist; (b) on each foot

Table 1 Main specifications of the 3D model of the proposed biped locomotor in Fig. 1

Parameter	Value
Degree of freedom	6 (3 per leg mechanism)
Weight	11.30 kg
Dimension (L×W×H)	500 mm×300 mm×502 mm
Step size	200 mm×40 mm
Step cycle	3 s/step
Speed	0.12 km/h

Table 2 Dimension parameters for the model in Fig. 3

Parameter	L	W	H	H_w	L_f	W_f	H_f	D_{uw}	D_{uf}	L_t	L_r	L_{i0}	H_f
Value/mm	500	300	502	10	201.6	126.6	10	35	35	263.6	317.4	435	10

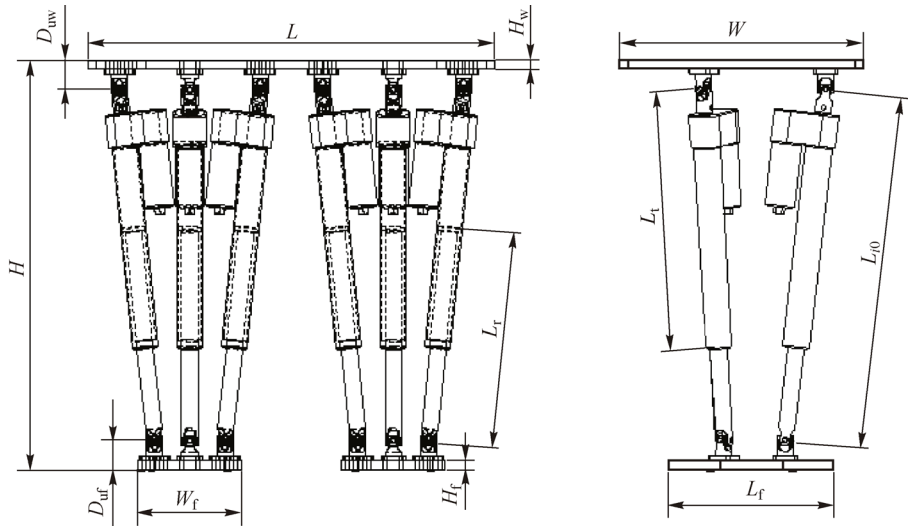

Fig. 3 Dimension parameters of the 3D model in Fig. 1 and Table 2

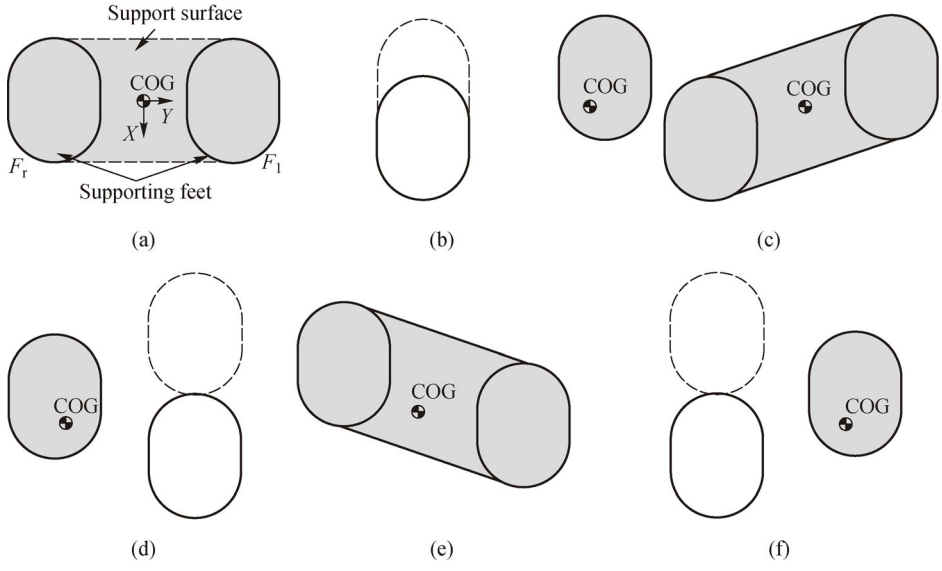

Fig. 4 A scheme for the motion planning of the biped walking gait in a horizontal plane: (a) Start and end configurations; (b) a half step for the start phase; (c) to (f) normal walking phases

In Fig. 4, the supporting feet that are in contact with the ground are indicated with gray color, while the swinging feet which are in the air are indicated with white color. The center of gravity (COG) of the locomotor indicates the projection of gravity center of the locomotor on the horizontal plane. The support surface is determined by using the supporting feet areas and is indicated with gray color. In Fig. 4(a), F_l and F_r represent the left and right feet, respectively, and the size of a foot is indicated by the dimension parameters L_f and W_f, as shown in Fig. 3 and Table 2. In Fig. 4, the biped walking gait is shown during six different phases by referring to double- and single-support phases. The double-support phase means that both feet are in contact with the ground as supporting feet, as shown in Figs. 4(a), 4(c), and 4(e), while the single-support phase means that either of the two feet swings in the air, and only one foot is in contact with the ground, as shown in Figs. 4(b), 4(d), and 4(f). The start/end configuration in Fig. 4(a) refers to both feet at rest and the start/end step is worked out as half of the full step. Figure 4(b) shows the feet positions at the start phase with half step ahead of one foot. The end configuration of the feet can be achieved similarly to the start phase with half step to reach the configuration in Fig. 4(b).

During biped walking gait, the human-like foot step trajectory of a reference foot point is an ovoid curve, which can be generated by using the Chebyshev mechanism [18], as shown in Fig. 5, where the straight line segment

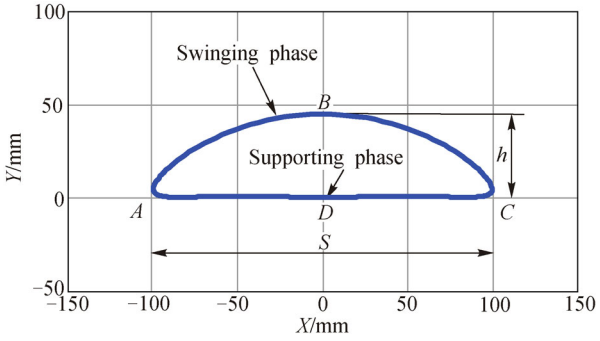

Fig. 5 Human-like foot step trajectory during biped walking gait

represents the supporting phase of the leg and the curve segment represents the swinging phase of the leg.

During the foot motion cycle, the foot step trajectory starts from Point *A* and follows the sequences of *A*-*B*-*C*-*D*-*A*. The step size can be characterized by a step length *s* and a step height *h*, which are assumed as $s = 200$ mm and $h = 40$ mm, as indicated in Table 1. In this case, the ratio between step height and length of human beings during normal walking is approximated with a ratio of the computed locomotor walker. In fact, the displacement along the *Y*-axis (step height *h*) is reasonable relative to the displacement along *X*-axis (step length *s*) in the proposed walking operation, because they have the values of $h = 40$ mm and $s = 200$ mm and it corresponds to a ratio of 0.2. However, it is possible to swing the foot at larger height to overpass obstacles like humans do. In addition, the start step in Fig. 4(b), which is a half step with $s' = 100$ mm, is performed by right foot. Both the start and end steps are half steps. The specified trajectories of the reference points for both left and right feet in 3D space are shown in Fig. 6.

Walking equilibrium is an important issue for biped locomotors, because they can only provide one or two feet in contact with the ground [19]. In general, there are two modes of walking for legged walking robots from equilibrium viewpoint, namely, static equilibrium walking and dynamic equilibrium walking [1]. Dynamic equilibrium walking can be achieved by controlling the ZMP (zero moment point) position of a robot to be inside the support polygon, thus allowing the robot to walk stably without unbalance configuration. The static equilibrium walking can be performed if-and-only-if the COG of a robot is projected vertically inside the support polygon [3]. Therefore, in order to achieve static equilibrium walking, the position COG is needed to be adjusted during the walking with proper foot size and leg motion. During the biped walking, the waist swinging can be used for COG position adjustment, as indicated in Fig. 6. A corresponding trajectory of the mass center (MC) of waist is indicated as a dashed line in Fig. 6.

In order to specify the motions of the waist and feet, the trajectories of their reference points are indicated as functions of time in Fig. 7 along the *X*-, *Y*- and *Z*-axes, respectively. In the plots, one can also see a standing-up period from $t = 0$ to 1 s, one half step at start phase from $t = 1$ to 4 s, and 4 steps during normal walking phases from $t = 4$ to 16 s. During the standing-up period, the waist and feet maintain the start configuration with constant values that represent the equilibrium of the biped locomotor before walking. Each step cycle of 3 s duration is divided into three segments, namely the first one from 0 to 0.75 s and last one from 2.25 to 3 s indicate the swinging motion of the waist during the double-support phase of the legs, and the middle segment from 0.75 to 2.25 s indicates the single-support phase of the legs.

4 Dynamic walking simulation

Dynamic walking simulation is carried out in MSC. ADAMS® environment to compute proper ground contact forces and actuator actions as functions of the prescribed

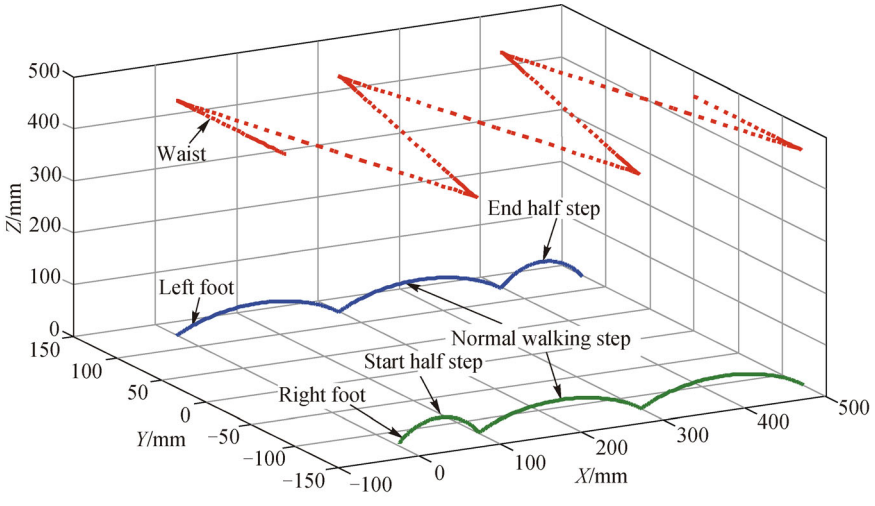

Fig. 6 Trajectories of the reference points for feet and waist in 3D space

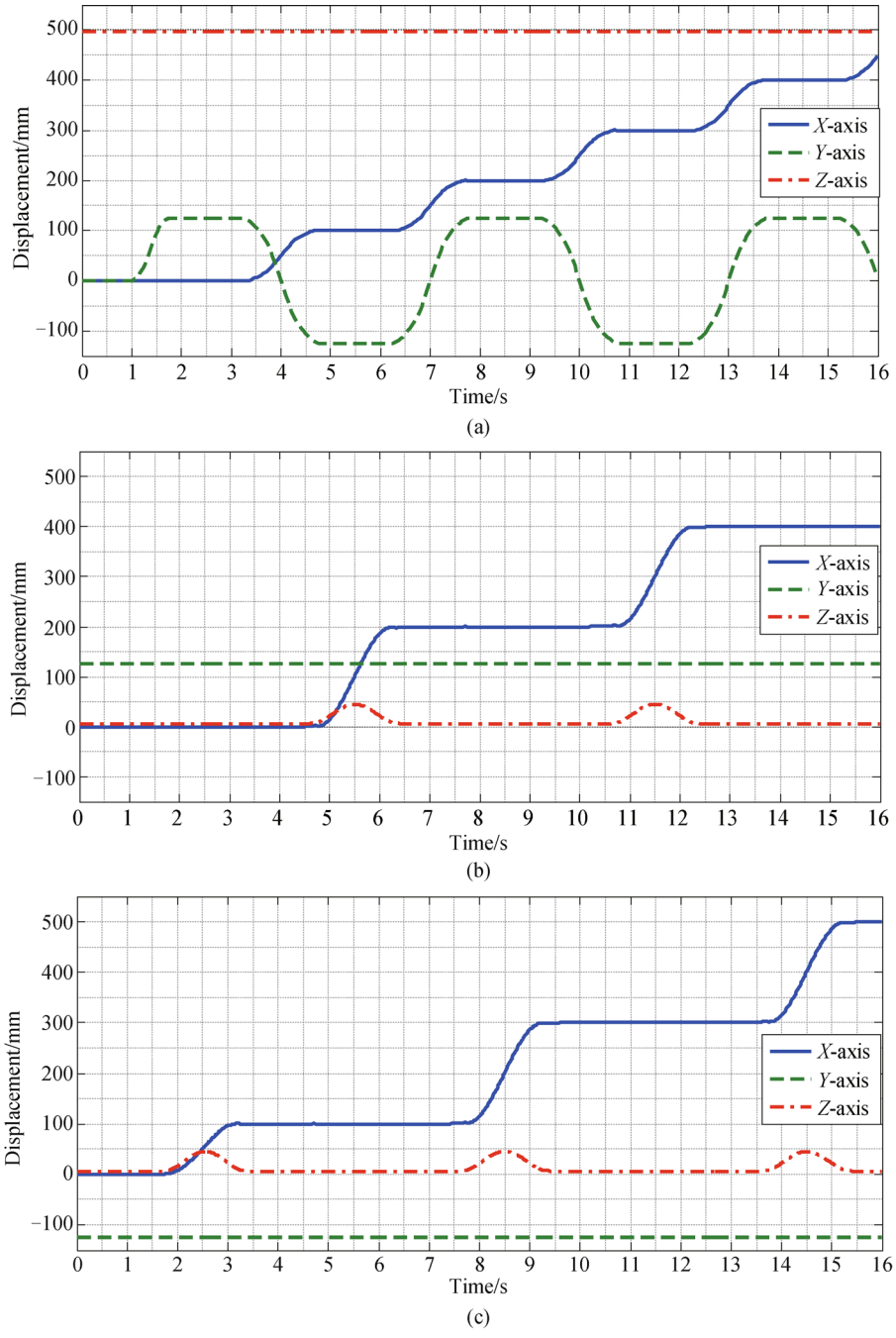

Fig. 7 Prescribed Cartesian components of the MC trajectories of: (a) The waist; (b) the left foot; (c) the right foot

human-like walking gait. A specific dynamic simulation procedure is proposed as summarized in Fig. 8; it consists of eight steps as indicated in Fig. 8.

Step 1: CAD modeling. In this phase, a 3D model of the proposed design is elaborated in SolidWorks® environment and then converted into Parasolid format (.x_t file). By importing the .x_t file into MSC.ADAMS® environment, a corresponding 3D model is created for numerical simulation in MSC.ADAMS® environment, as shown in Fig. 9. A reference system is fixed on the ground as a world frame, where the origin is located at the projection of COG, the *X*-axis indicates the forward direction, and the *Z*-axis indicates the upward direction, as shown with an enlarged view in Fig. 9.

Step 2: Setup of material properties and constraints. Material property is assumed for each part by using the default data of certain materials, and constraints are expressed between parts to achieve desired motions. In particular, the calculated mass values of each component are listed in Table 3, which presents m_w for the waist, m_f for

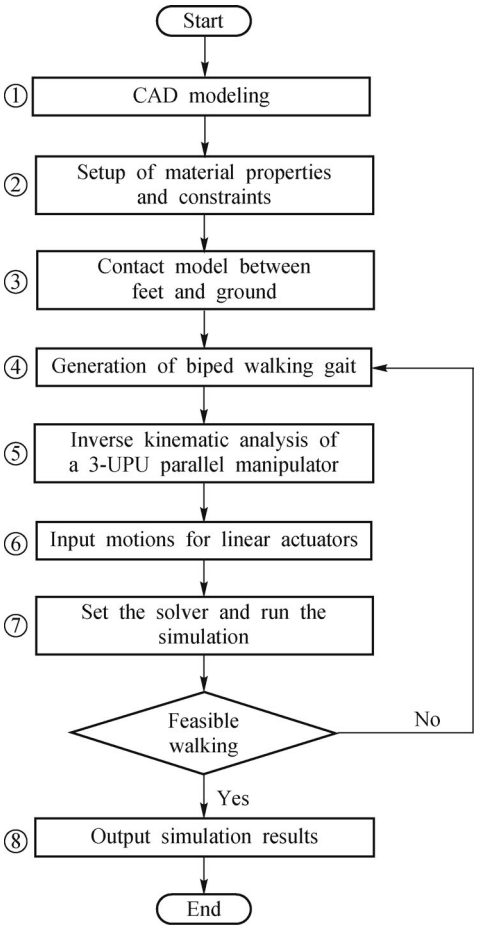

Fig. 8 Flowchart of the dynamic simulation procedure

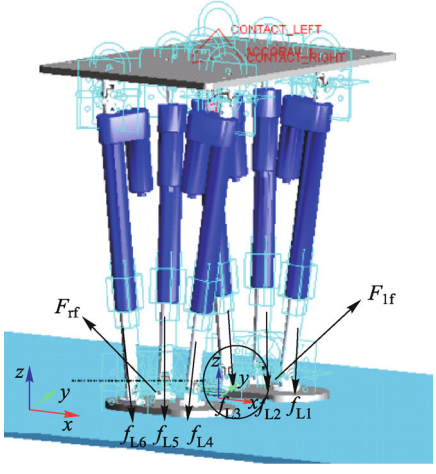

Fig. 9 A 3D dynamic model of the biped locomotor with characteristic forces in MSC.ADAMS® environment

one foot, m_{lt} for one tube, m_{lr} for one rod, and m_{Uj} for one U-joint. The mass value of one leg (m_{leg}) can be calculated as

$$m_{leg} = 3(m_{lt} + m_{lr} + 2m_{Uj}) + m_f, \quad (5)$$

with the consideration that each limb of one tripod leg mechanism is made up of one tube frame body, a sliding rod, and two U-joints.

Step 3: Contact model between feet and ground. 3D solid contact constraints are assumed for simulating the contact conditions between the feet and the ground. Normal force is modelled by using the impact function model, which is based on the Hertzian contact theory, while friction is modelled by using a Coulomb friction model. Values of the coefficients are determined based on material properties (Young's modulus and Poisson's ratio) and geometrical properties (radius of curvature) [20]. These values are assumed as 0.4 for static friction coefficient, 0.1 for dynamic friction coefficient, 10.0 N·s/mm for damping coefficient, and 1.0×10^4 N/mm for stiffness at the contact.

Step 4: Generation of the biped walking gait. The biped walking gait is generated by specifying the swinging of the waist and step size of the feet, as discussed in Section 3.

Step 5: Inverse kinematic analysis of a 3-UPU parallel manipulator. The displacement of each linear actuator is calculated based on the inverse kinematic analysis indicated in Section 2 and the generated biped walking gait discussed in Section 3.

Step 6: Input motions for linear actuators. The previously calculated data are imported into MSC.ADAMS® environment by using the spline function, after which the motion elements are added to the prismatic constraints of linear actuators. The calculated input displacements of the rod of each linear actuator are plotted in Fig. 10 as function of time. During normal walking, the displacements of L4 and L1, L5 and L3, and L6 and L2 are similar to one another with one step delay because of the prescribed walking gait and structure symmetry.

Step 7: Set the solver and run the simulation. The solver is set by using the default WSTIFF integrator with SI2 formulation. In MSC.ADAMS® environment, simulation time of the walking is fixed to 16 s to simulate four normal walking steps (3 s/step) and one start half start step (3 s/step). Computation interval time is set as 0.005 s in order to ensure feasible numerical solutions in the simulation run.

Step 8: Output simulation results. In the postprocessor, simulation results are given in proper form for further analysis.

Table 3 Mass values of components for the 3D model in Fig. 9

Parameter	m_w	m_f	m_{lt}	m_{lr}	m_{Uj}	m_{leg}	Total mass
Value/kg	4.08	0.61	0.68	0.22	0.05	3.61	11.30

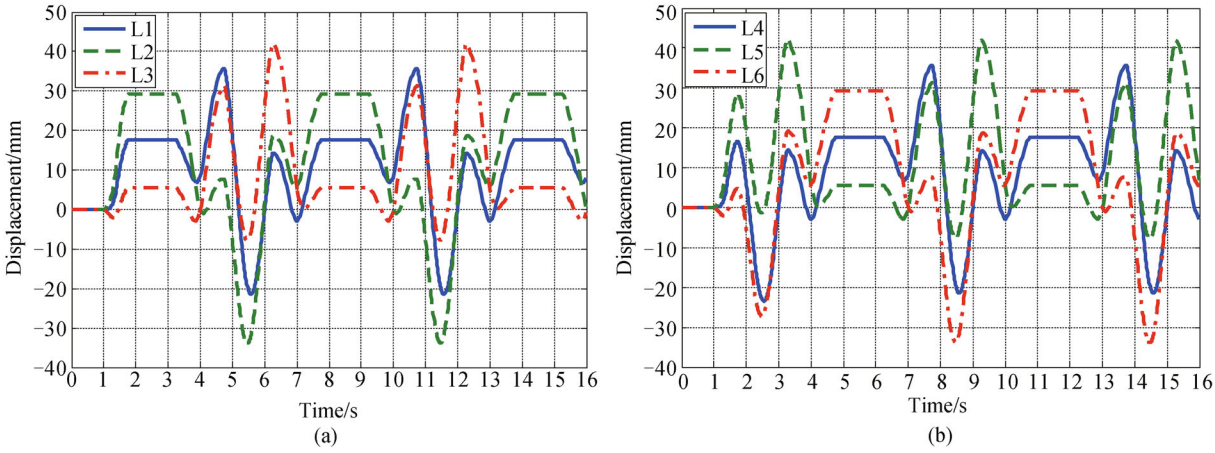

Fig. 10 Input displacements of the six linear actuators in the MSC.ADAMS® environment for: (a) Left leg; (b) right leg

5 Simulation results

Simulation results are presented in terms of the computed actuation forces for six linear actuators, contact forces between feet and ground, linear accelerations of the waist and two feet, and the trajectories of the waist and feet. These results can be considered as performance characteristics for evaluating a practical feasible operation of the proposed biped locomotor.

The computed actuation forces of the six linear actuators are reported in Fig. 11. The respective time histories of f_{L1} and f_{L4}, f_{L2} and f_{L6}, f_{L3} and f_{L5} are similar to one another with one step delay as due to the coordination of leg motion during the normal walking. In each tripod leg mechanism, the force value of the front linear actuator (f_{L1} or f_{L4}) is much less than the values in the other two rear ones (f_{L2} and f_{L3} or f_{L5} and f_{L6}), as a consequent of the leg structure and proposed planning of walking gait with waist swinging. In addition, the maximum values always occur at the start or end of each foot step because of the feet leaving from or landing on the ground, namely, when changing status between double-support and single-sup-

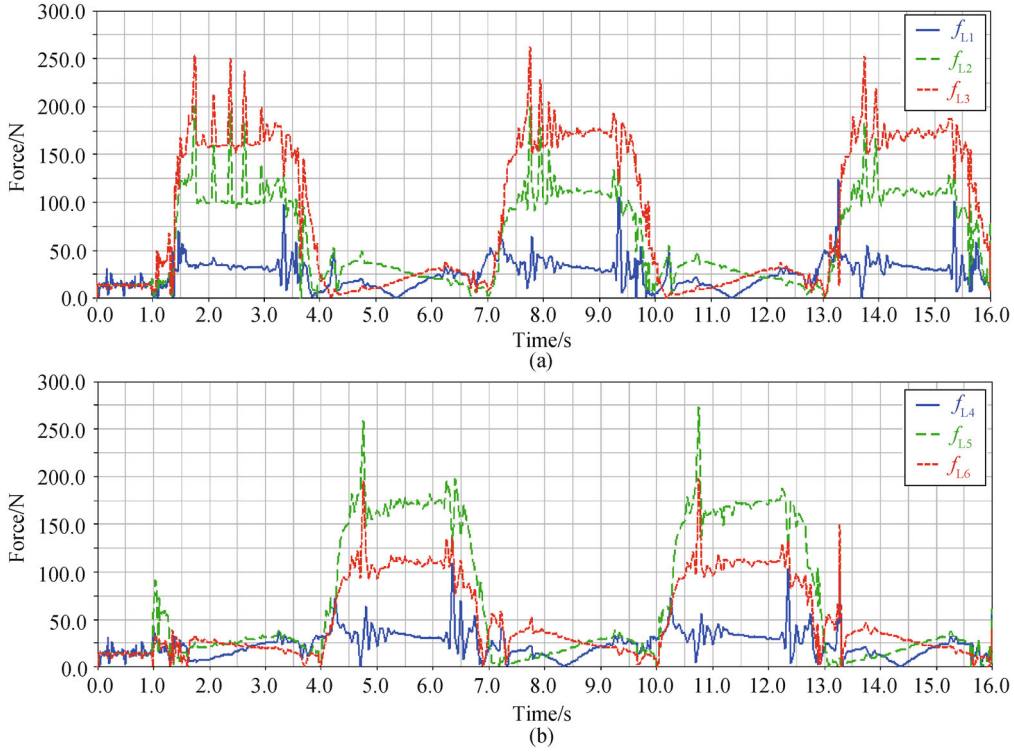

Fig. 11 Computed input actuation forces of the six linear actuators: (a) Left leg; (b) right leg

port phases. The peak values of forces f_{Li} ($i = 1, 2, \ldots, 6$) are computed as 124.35 N, 196.93 N, 274.35 N, 109.58 N, 274.83 N, 196.26 N, respectively. They can be considered proper values and are also useful for selecting actuators with suitable sizes and output power from market available solutions.

For biped locomotors, the contact forces between the feet and the ground should be maintained within proper values, otherwise too large contact forces could deteriorate the walking equilibrium of the biped locomotor up to even damage the mechanical structure. Figure 12 shows the computed contact forces of the two feet along the *X*-, *Y*-, and *Z*-axes, respectively. The *Z*-axis component of contact forces (normal force) is much larger than the other two components that are mainly related to friction actions. There are one or two minor jumps in each step, which are due to the corresponding foot landing impact on the ground and the waist swinging. The peak values are computed less than 125 N, and the average values are computed of about 110 N. Those values can be considered reasonable for the weight of the biped locomotor. The double-support phase and single-support phase can be also identified by the contact forces in Fig. 12, as indicated by the characteristics Points *E* to *I*. The intervals *EF* and *GH* refer to double-support phases, and intervals *FG* and *HI* refer to single-support phases. The walking equilibrium can be also observed from the values of normal forces which are relatively constant during single-support phases and smoothly change during the double-support phases.

Figure 13 shows the computed MC linear accelerations of the waist and feet along the *X*-, *Y*-, and *Z*-axes, respectively. As can be seen, the *X*-axis and *Y*-axis components of the waist MC acceleration are much larger than the *Z*-axis component, and the *X*-axis and *Z*-axis components of the foot MC accelerations are much larger than the *Y*-axis component. In particular, in Figs. 13(b) and 13(c), the *Y*-axis component of foot acceleration values is approximately equal to zero, and in each step cycle, the *X*- and *Z*-axes components increase first and then decrease. These results are in agreement with the prescribed motion of the waist and feet presented in Fig. 7. In addition, there are one or two jumps in each step, which are due to the corresponding foot landing impact on the ground and the waist swinging. The maximum peak values of the motions for the waist and feet have been computed to be less than 6 and 8 m/s^2, respectively. These values can be considered feasible values when they are compared with the strike acceleration in human heel during a normal walking, which generally gives values larger than 50 m/s^2 [21].

In Fig. 14, the computed trajectory of the waist MC is plotted in the *O*-*XY* and *O*-*XZ* planes, respectively. The computed Cartesian components of the MC trajectories of the waist and feet are indicated as functions of time in Fig. 15 along the *X*-, *Y*- and *Z*-axes, respectively. In Fig. 14, the normal walking step length *s* is computed to be approximately equal to 200 mm, which corresponds to the prescribed step size as indicated in Table 1. The jumps in the *O*-*XZ* plane always occur when the displacement of

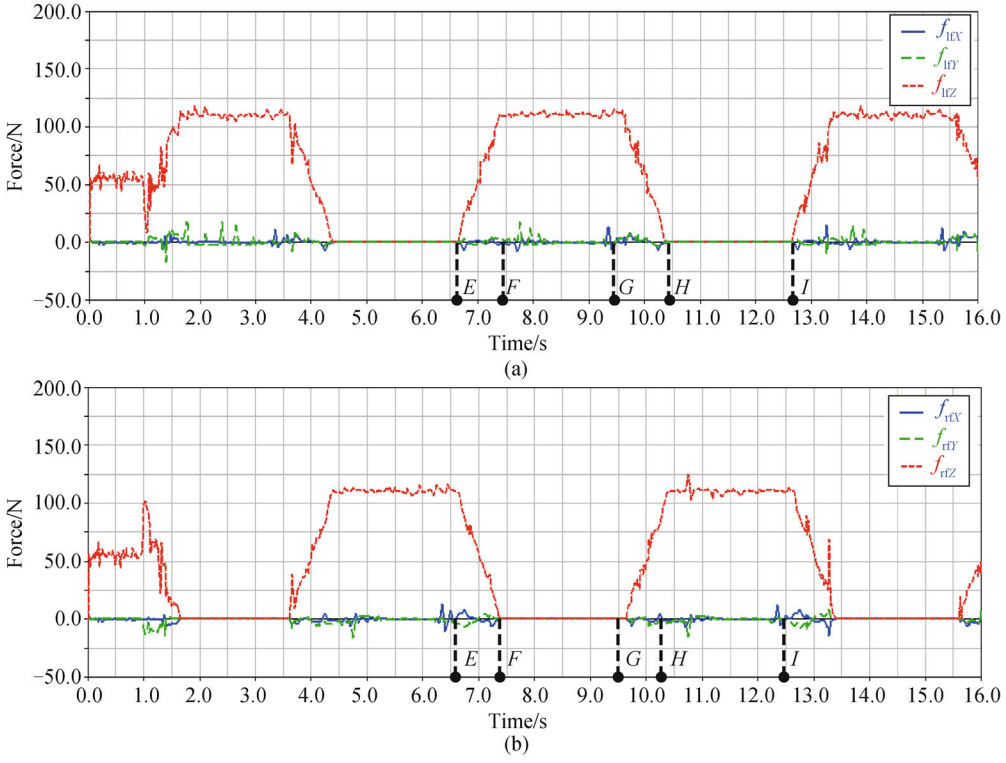

Fig. 12 Computed contact forces between the feet and the ground: (a) Left foot; (b) right foot

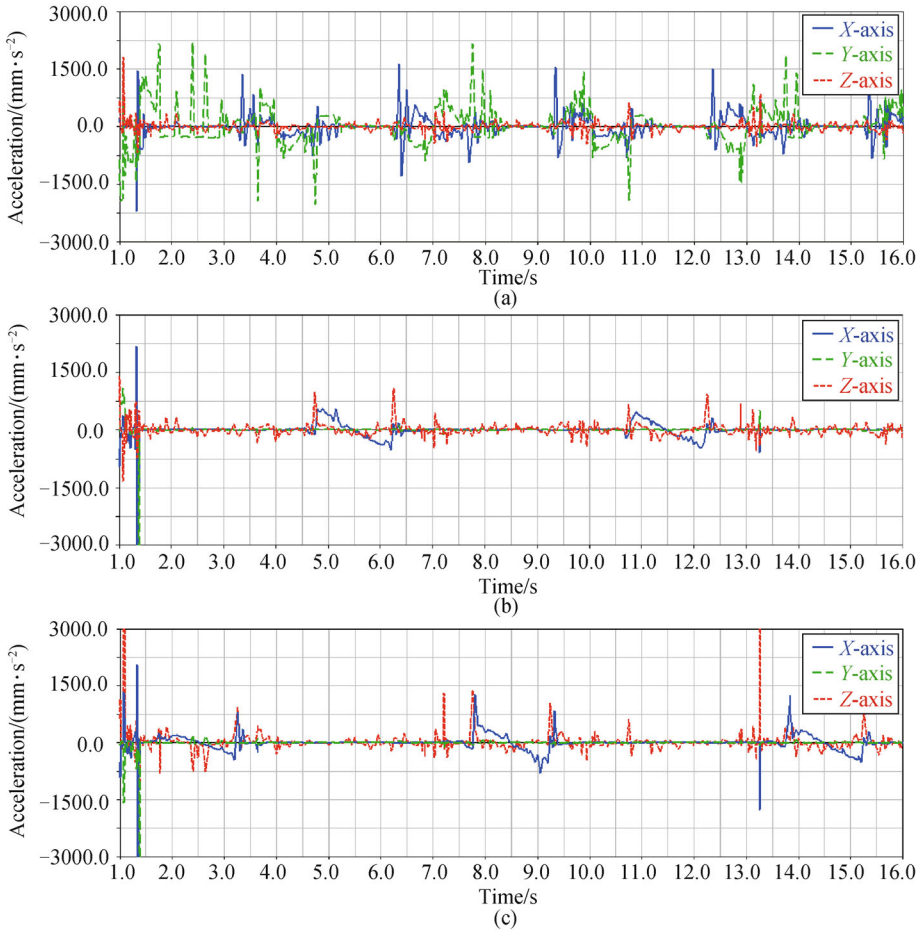

Fig. 13 Computed MC linear accelerations during the walking for: (a) Waist; (b) left foot; (c) right foot

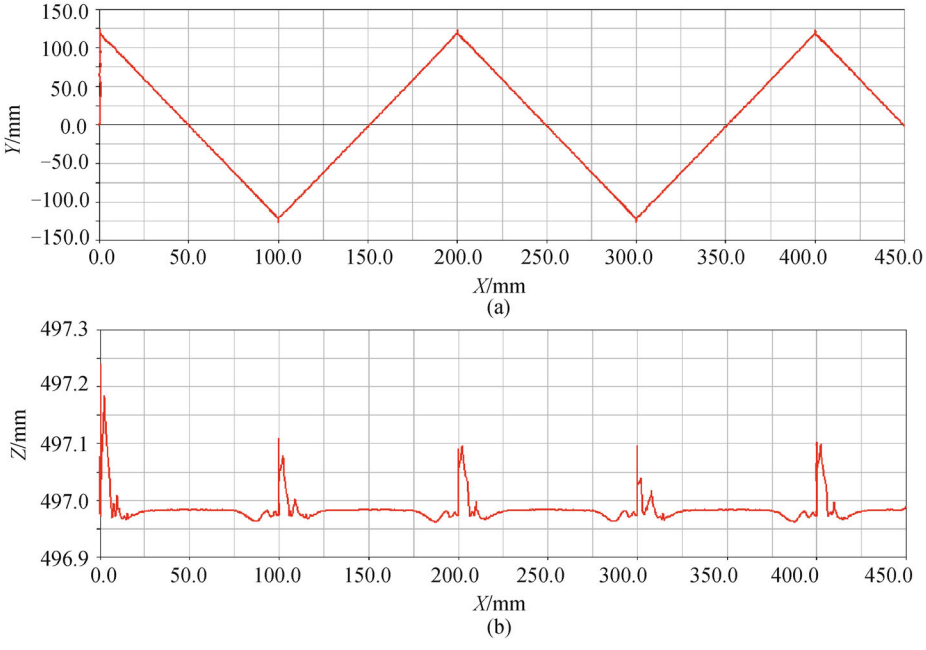

Fig. 14 Computed MC trajectory of the waist: (a) In the *O-XY* plane; (b) in the *O-XZ* plane

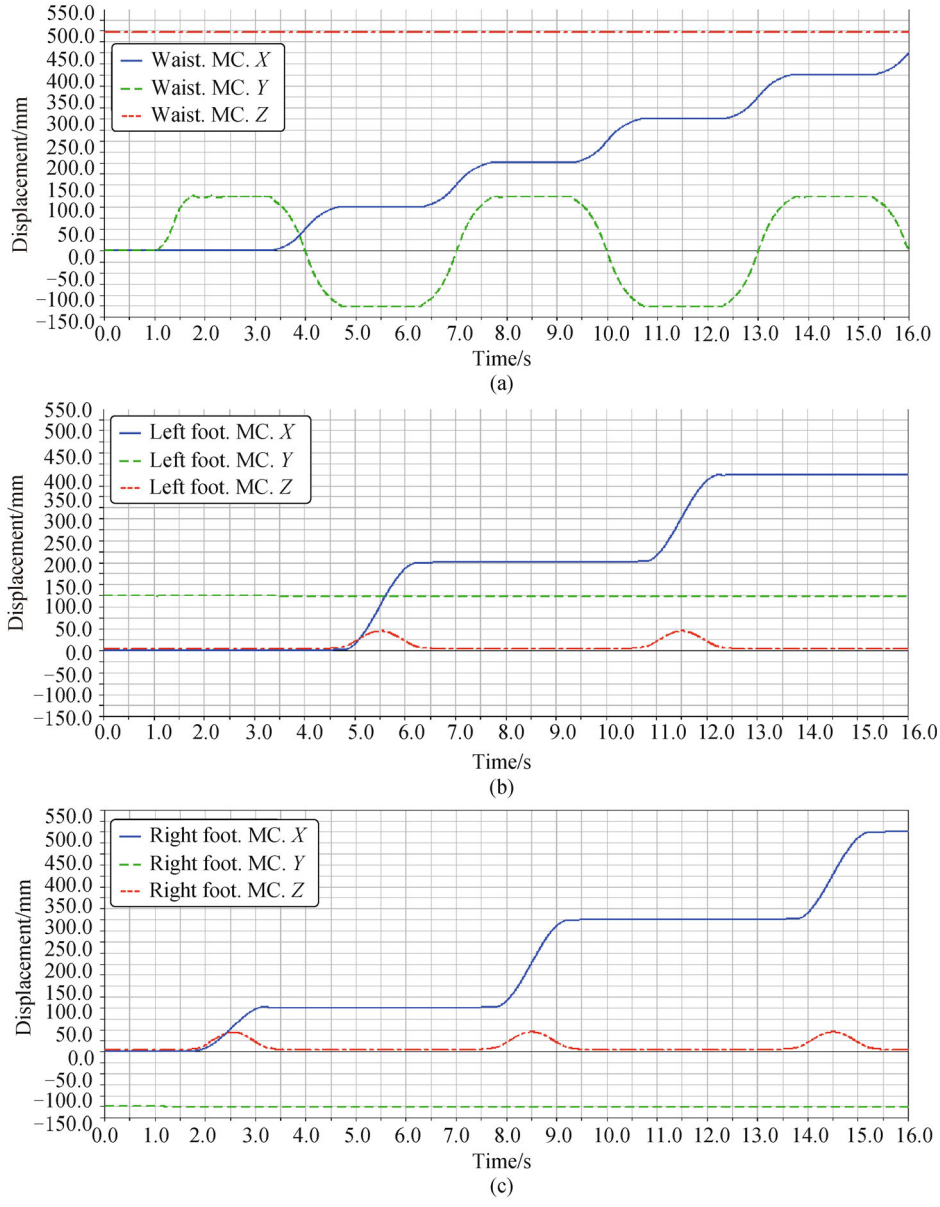

Fig. 15 Computed Cartesian components of the MC trajectories of: (a) Waist; (b) left foot; (c) right foot

the waist MC equals 0, 100, 200, 300, or 400 mm along *X*-axis and the maximum value has been computed to be less than 0.3 mm. By considering Fig. 15, it can be noted that the jumps occur in two situations, namely, a first one when the waist stops swinging while one foot leaves the ground, and a latter one when one foot lands on the ground while the waist starts swinging. In this case, these jumps are caused by the swinging motion of the waist and the impact of the foot landing on the ground.

In order to clearly present the effect of the waist swinging and contact impact for the overall walking operation, the computed difference of the Cartesian components between the prescribed and simulated MC trajectories of the waist and feet is reported in Fig. 16. The waist drift and the foot slipping are respectively characterized during the start step and 4 normal steps. During the start step, namely from 1 to 4 s, the drift displacement of the waist reaches a maximum of 0.42 mm along the *X*-axis and 1.89 mm along the *Y*-axis, corresponding to swinging displacements of 50 and 125 mm along the *X*- and *Y*-axes, respectively. In addition, the slipping displacement of the foot reaches a maximum of 0.26 mm along the *X*-axis and 0.76 mm along the *Y*-axis, corresponding to the foot step displacement of 200 mm along the *X*-axis and a swing displacement of 125 along the *Y*-axis. Two large slipping motions occur during this period, one is due to the waist swings from the start configuration to left side, and the other one is due to the waist swinging from the left side to right side. During the 4 normal steps, namely from 4 to 16 s, the drift displacement of the waist reaches a maximum of

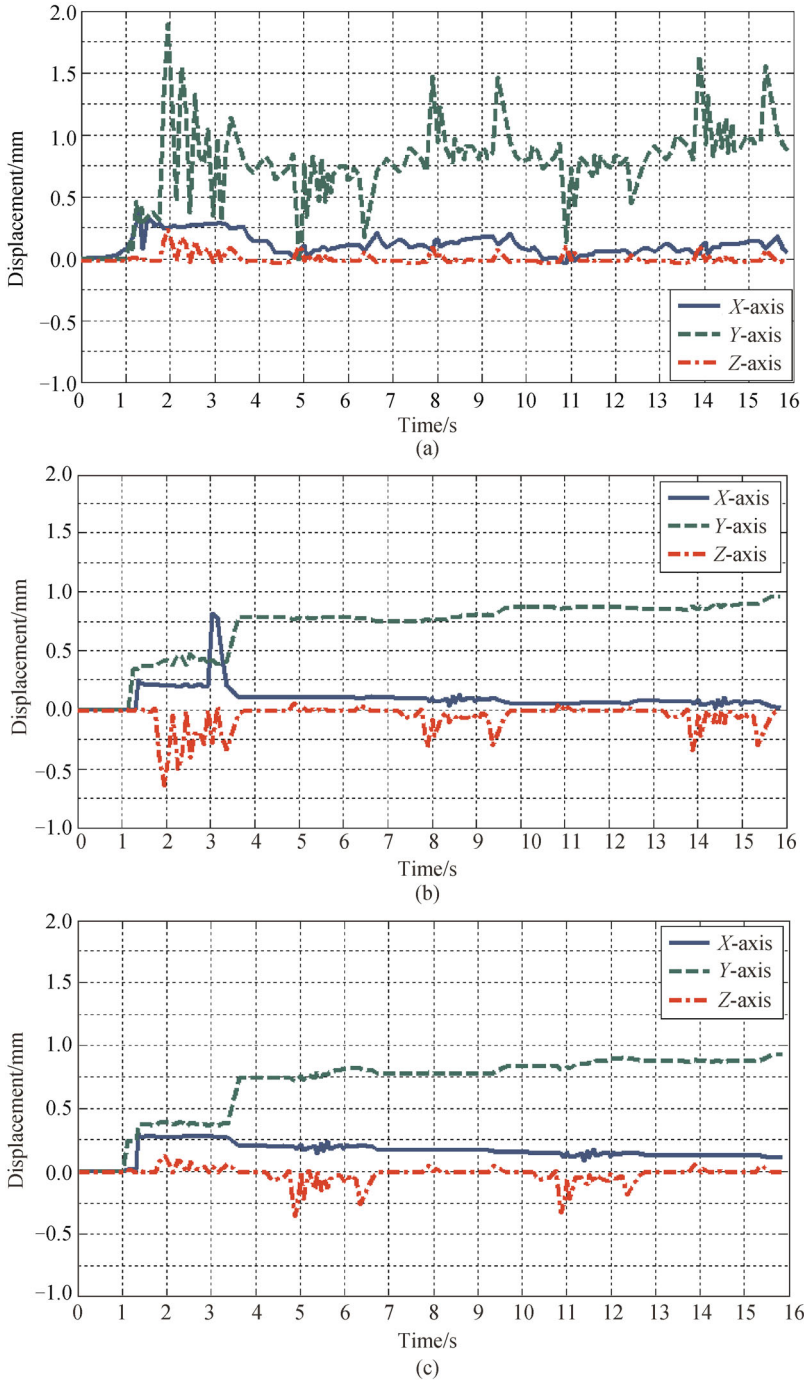

Fig. 16 Difference between the prescribed and computed displacements of the MCs of: (a) Waist; (b) left foot; (c) right foot

0.21 along the *X*-axis and 0.78 mm along the *Y*-axis only, and it is much smaller than the corresponding swinging displacement of 400 mm along *X*-axis and 125 mm along the *Y*-axis. The slipping displacement of the foot reaches a maximum of 0.09 mm along the *X*-axis and 0.11 mm along the *Y*-axis only, and it is much smaller than the corresponding displacements in the footsteps of 400 mm and in the waist swinging of 125 mm. Hence, the proposed locomotor walks with insignificant values of the waist drift and foot slipping during normal walking.

Figure 17 shows the snapshots of the simulated biped walking sequences that correspond to the phases of the biped walking gait in Fig. 4. The MC trajectories of the waist and feet are slightly marked with continuous lines. The designed biped locomotor walks on the ground with a desired biped walking gait, when waist swinging is

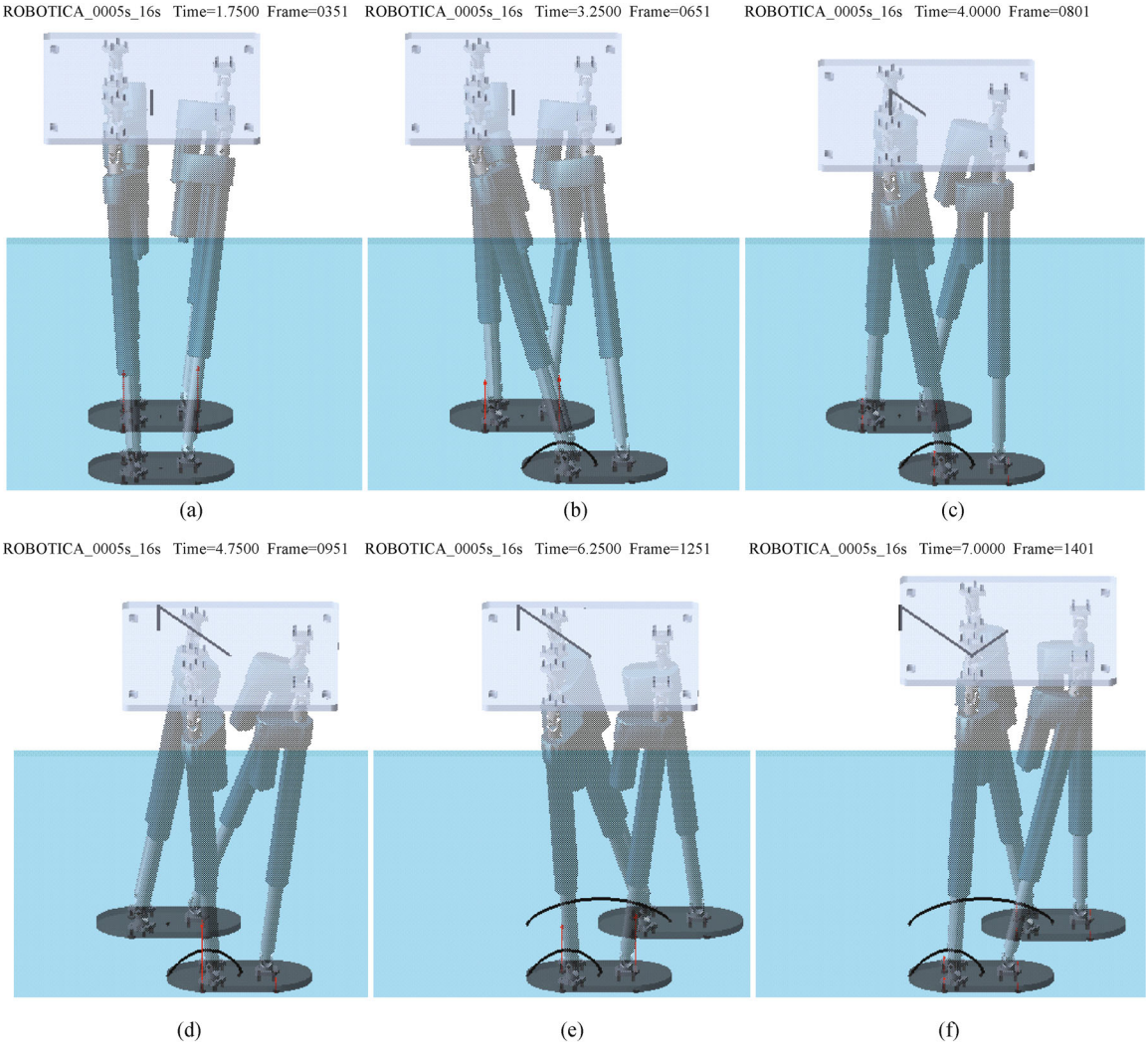

Fig. 17 Snapshots of the simulated biped walking sequences of the tripod leg mechanism locomotor in MSC.ADAMS® environment, referring to the walking gait in Fig. 4. (a) $t = 1.75$ s; (b) $t = 3.25$ s; (c) $t = 4.0$ s; (d) $t = 4.75$ s; (e) $t = 6.25$ s; (f) $t = 7$ s

coordinated with the motion of the two tripod leg mechanisms to keep the equilibrium of the locomotor during biped walking.

6 Preliminary test

In Fig. 18, a preliminary prototype of the Cassino biped

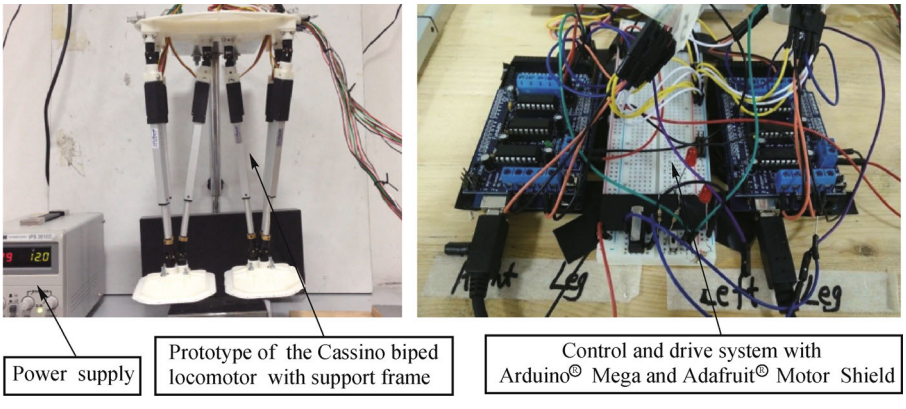

Fig. 18 Layout for the proposed biped locomotor for experimental tests in air

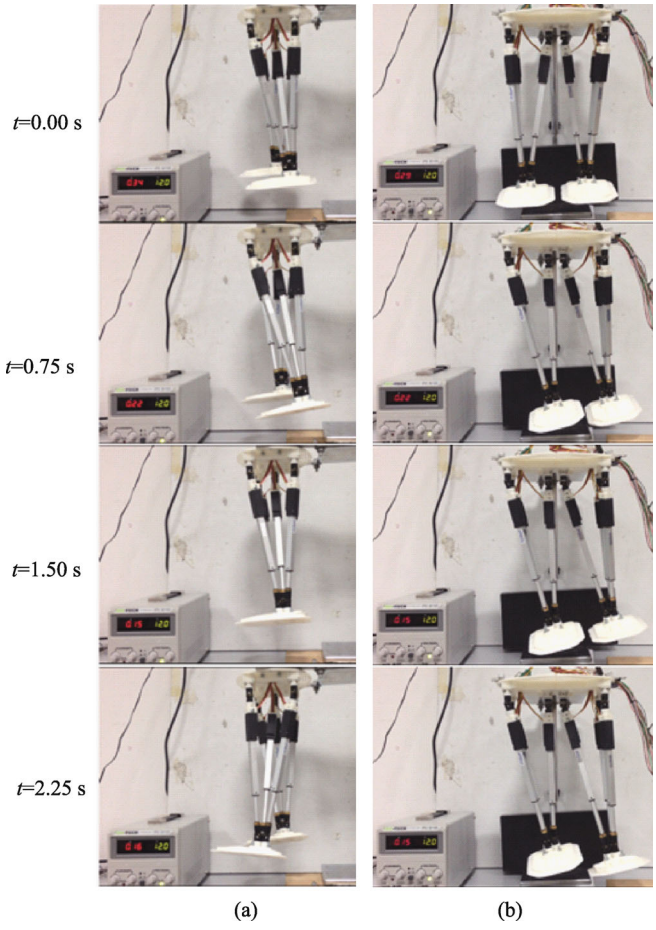

Fig. 19 Snapshots of a normal walking step sequences in the air: (a) In the sagittal plane, (b) in the frontal plane

locomotor is built with the control system for testing the proposed walking operation in the air. Each leg mechanism is actuated by three linear actuators with 12 V DC motors, which are controlled by an Adafruit® Motor Shield with instructions from an Arduino® Mega based on PID control strategy. Specifically, each linear actuator is driven to follow the prescribed input displacement as shown in Fig. 10 under a PID closed loop control. In Fig. 19, a sequence of biped locomotor configurations during a normal walking step is respectively shown in the sagittal and frontal planes with the corresponding test time. The experimental test results show that the built preliminary prototype can perform a predefined biped walking gait in the air, which is quite useful for identifying the operation performance of the prototype, validating the mechanical design, and looking for enhancements.

7 Conclusions

A mechanical design of a Cassino biped locomotor with two tripod leg mechanisms is presented through a dynamic simulation of its characteristic biped walking. A 3D model has been elaborated in SolidWorks® environment for evaluating design performance and checking the operation feasibility. A planning of biped walking gait has been proposed by properly operating waist swinging in coordination with the two leg motions. Then, dynamic simulation has been carried out in MSC.ADAMS® environment to compute proper ground contact forces and actuator actions as a function of human-like input motion. Results show that the proposed biped locomotor with prescribed walking gait gives limited reaction forces between the feet and ground, and has a practical feasible walking ability on flat surfaces. Test results of the preliminary prototype have validated the feasibility of the proposed biped locomotor with the planned biped walking operation in the air.

Acknowledgements The first author acknowledges the Chinese Scholarship Council (CSC) for supporting his PhD study and research at the Laboratory of Robotics and Mechatronics (LARM) at the University of Cassino and South Latium, Italy, during the years 2013–2015.

References

1. Pfeiffer F. Technological aspects of walking. In: Pfeiffer F, Zielińska T, eds. Walking: Biological and Technological Aspects. New York:

Springer, 2004, 119–153
2. Carbone G, Ceccarelli M. Legged Robotic Systems. Cutting Edge Robotics. Vienna: ARS Scientific Book, 2005, 553–576
3. Siciliano B, Khatib O. Springer Handbook of Robotics. Berlin: Springer, 2008, 361–390
4. Sakagami Y, Watanabe R, Aoyama C, et al. The intelligent ASIMO: System overview and integration. In: Proceedings of 2002 IEEE/RSJ International Conference on Intelligent Robots and Systems (IROS'02). Lausanne: IEEE, 2002, 3: 2478–2483
5. Park I W, Kim J Y, Lee J, et al. Mechanical design of humanoid robot platform KHR-3 (KAIST humanoid robot-3: HUBO). In: Proceedings of IEEE/RAS International Conference on Humanoid Robots (Humanoids'05). Tsukuba: IEEE, 2005, 321–326
6. Kaneko K, Kanehiro F, Kajita S, et al. Design of prototype humanoid robotics platform for HRP. In: Proceedings of IEEE/RSJ International Conference on Intelligent Robots and Systems (IROS'02). Lausanne: IEEE, 2002, 3: 2431–2436
7. Ceccarelli M. Fundamentals of Mechanics of Robotic Manipulation. Dordrecht: Kluwer Academic Publishers, 2004
8. Merlet J P. Parallel Robots. 2nd ed. Dordrecht: Springer, 2006
9. Hashimoto K, Sugahara Y, Lim H O, et al. Biped landing pattern modification method and walking experiments in outdoor environment. Journal of Robotics and Mechatronics, 2009, 20(5): 775–784
10. Wang H, Qi Z, Hu Z, et al. Application of parallel leg mechanisms in quadruped/biped reconfigurable walking robot. Journal of Mechanical Engineering, 2009, 45(08): 24–30 (in Chinese)
11. Ceccarelli M, Carbone G. A new leg design with parallel mechanism architecture. In: Proceedings of 2009 IEEE/ASME International Conference on Advanced Intelligent Mechatronics (AIM'09). Singapore: IEEE, 2009, 1447–1452
12. Pan Y, Gao F. Payload capability analysis of a new kind of parallel leg hexapod walking robot. In: Proceedings of 2013 International Conference on Advanced Mechatronic Systems (ICAMechS'13). Luoyang: IEEE, 2013, 541–544
13. Wang M, Ceccarelli M. Design and simulation for kinematic characteristics of a tripod mechanism for biped locomotors robots. In: Proceedings of International Workshop on Robotics in Alpe-Adria-Danube Region (RAAD'13). Portorož, 2013, 124–131
14. Wang M, Ceccarelli M, Carbone G. Experimental tests on operation performance of a LARM leg mechanism with 3-DOF parallel architecture. Mechanical Sciences, 2015, 6(1): 1–8
15. Joshi S, Tsai L W. A comparison study of two 3-DOF parallel manipulators: One with three and the other with four supporting legs. IEEE Transactions on Robotics and Automation, 2003, 19(2): 200–209
16. Bhutani G, Dwarakanath T A. Practical feasibility of a high-precision 3-UPU parallel mechanism. Robotica, 2014, 32(3): 341–355
17. Dehkordi M B, Frisoli A, Sotgiu E, et al. Modelling and experimental evaluation of a static balancing technique for a new horizontally mounted 3-UPU parallel mechanism. International Journal of Advanced Robotic Systems, 2012, 9(193): 1–12
18. Liang C H, Gu H, Ceccarelli M, et al. Design and operation of a tripod walking robot via dynamics simulation. Robotica, 2011, 29 (05): 733–743
19. Huston R L. Principles of Biomechanics. Boca Raton: CRC Press, 2009, 344–347
20. Adams G G, Nosonovsky M. Contact modeling—Forces. Tribology International, 2000, 33(5–6): 431–442
21. Rose J, Gamble J G. Human walking. 3rd ed. Philadelphia: Lippincott Williams & Wilkins, 2005